RESEARCH ARTICLE | NOVEMBER 21 2023

Highly efficient removal of bubbles from water pipes by femtosecond laser-designed superhydrophobic porous microstructures

Yansheng Yao ; Qiangsong Meng ; Yubin Peng ; Zilong Cheng; Xinlei Li; Tianyu Xu; Jiale Yong

Appl. Phys. Lett. 123, 211601 (2023)
https://doi.org/10.1063/5.0171357

Applied Physics Letters ARTICLE pubs.aip.org/aip/apl

Highly efficient removal of bubbles from water pipes by femtosecond laser-designed superhydrophobic porous microstructures

Cite as: Appl. Phys. Lett. **123**, 211601 (2023); doi: 10.1063/5.0171357
Submitted: 8 August 2023 · Accepted: 7 November 2023 ·
Published Online: 21 November 2023

Yansheng Yao,[1] Qiangsong Meng,[1] Yubin Peng,[1,a)] Zilong Cheng,[2] Xinlei Li,[2] Tianyu Xu,[2] and Jiale Yong[2,a)]

AFFILIATIONS

[1]Intelligent Manufacturing Laboratory, School of Mechanical and Electrical Engineering, Anhui Jianzhu University, Hefei 230009, China
[2]Department of Precision Machinery and Precision Instrumentation, University of Science and Technology of China, Hefei, 230027, China

[a)]**Authors to whom correspondence should be addressed:** pengyubin@ahjzu.edu.cn and jlyong@ustc.edu.cn

ABSTRACT

Here, we propose a strategy that combines a superhydrophobic surface microstructure with perforated microholes prepared by femtosecond laser processing to efficiently remove bubbles in water pipes. Driven by Laplace pressure and underwater pressure, the bubbles in water are easily absorbed by the superhydrophobic porous thin tube and then discharged into the external air environment. The gas discharge rate of the superhydrophobic porous film is approximately seven times that of the ordinary porous film. Inserting a superhydrophobic porous thin tube in the infusion tube allows entire bubbles to be completely discharged out of the infusion tube. The method of removing bubbles in water based on superhydrophobic porous tubes will have important applications in microfluidic, biomedical, and chemical manufacturing and can effectively avoid the harm caused by tiny bubbles.

There are inevitably tiny bubbles in the water. Although bubbles can sometimes be used to improve water quality,[1] generate electricity,[2] etc., undesirable bubbles in the water flow often have a negative effect on thin water pipes.[3–6] Tiny bubbles in the microchannel will attach to the inner wall of the pipe [Fig. 1(a)]. Even small bubbles can increase fluid resistance and even block microchannels.[7–10] Injecting air bubbles into the human body through a medical infusion tube is one of the main causes of many medical accidents caused by air embolism.[11–13] The air–blood interaction induces the formation of fibrin clots or blood clots, which impede the normal circulation of blood. Effectively removing bubbles in water pipes is an effective way to avoid the above problems.[14–16] Traditional methods for removing tiny bubbles from liquids are based on ultrasonic degassing, heating boiling, adding an elimination agent, and so on.[6,15,17] However, these operations often require additives or complex equipment and require external energy input. To date, developing a simple and environmentally friendly strategy to achieve effective water/gas separation has remained challenging but highly anticipated. Recently, Yong *et al.* found that the wettability of porous structures plays a decisive role in the permeation behavior of underwater bubbles through porous membranes.[18–21] The underwater bubbles can easily pass through the superhydrophobic and superaerophilic porous films but will be intercepted by the superhydrophilic and superaerophobic porous films. The effect of surface wettability on bubble permeability provides a new strategy for removing tiny bubbles in water flow.[5,6,22,23] As shown in Fig. 1(b), a superhydrophobic porous thin tube is inserted into the water pipe. Bubbles in the water flow can be adsorbed by the inserted tube and further released into the external environment through the tube. The porous thin tube needs to have properties that allow air bubbles to enter its interior and repel water.

In this Letter, the effects of femtosecond laser-induced superhydrophobic microstructures and perforated microholes on the permeability of underwater bubbles are investigated. The results show that both the superhydrophobic microstructure and the microholes on the polytetrafluoroethylene (PTFE) film play an important role in the rapid adsorption of underwater bubbles, the bubbles passing through the film, and the release of gas into the external environment. When superhydrophobic porous microstructures are prepared on the wall of thin tubes, the tubes can be used to remove bubbles from water. An efficient bubble removal strategy based on a superhydrophobic porous

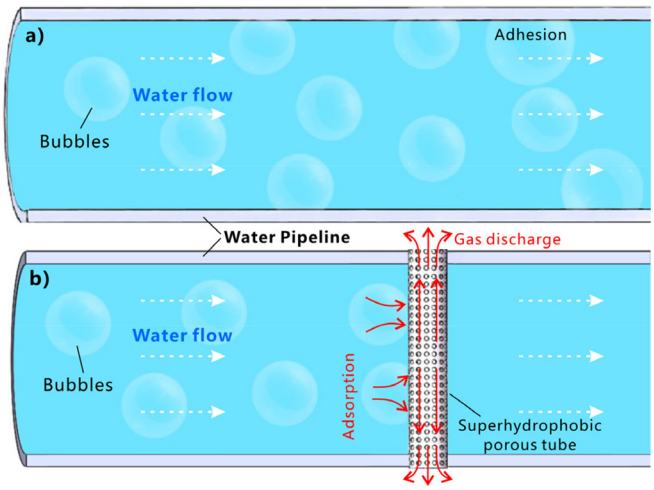

FIG. 1. Schematic diagram of a strategy to remove bubbles from the water flow in a pipeline. (a) Bubbles attached to the wall of the normal water pipe. (b) Inserting a superhydrophobic porous gas tube into the water pipeline to absorb the bubbles and release them to the external environment.

tube is proposed to prevent bubbles from being injected into the human body.

The ultrashort pulse width and ultrahigh peak power have made femtosecond (10^{-15} s) lasers one of the most important tools in modern extreme and ultraprecision manufacturing.[24–26] The desired superhydrophobic porous microstructure can be prepared on a PTFE film/tube using a femtosecond laser due to its ability to simultaneously generate micro/nanoscale surface structures and open microholes. As shown in Fig. 2(a), the laser beam (pulse width = 35 fs, wavelength = 800 nm, repetition rate = 1 kHz) enters the scanning galvanometer and is further focused on the PTFE surfaces by the f–θ lens (focal length = 100 mm). The galvanometer controls the scanning path. Typically, a uniform microstructure can be prepared on the substrate surface by classical line-by-line scanning [Fig. 2(b)]. Figure 2(d) shows the scanning electron microscopy (SEM) image of the PTFE surface that was ablated by a femtosecond laser at a laser power (Ω) of 50 mW, scanning speed (v) of 10 mm/s, and scanning space (Λ) of 20 μm. The surface is coated with a large number of hierarchical pores and protrusions, with protrusion sizes ranging from 300 nm to 2 μm.

Figure S1 (supplementary material) shows the x-ray photoelectron spectroscopy (XPS) of the original and laser treated PTFE surface. The chemical elements C, O, and F are detected on both untreated and treated surfaces [Fig. S1(a), supplementary material]. It is found that the signal strength of the O element after laser treatment is significantly higher than that on the untreated PTFE surface, and the atomic percentage of O element increases obviously after laser treatment (Table S1, supplementary material). To further explore the change in chemical components, the narrow scan spectra of C1s, O1s, and F1s are peak-fitted in Figs. S1(b)–S1(d) in the supplementary material. It can be found that the difference in chemical component before and after laser treatment is mainly concentrated in C–O. The C–O of original PTFE may come from the adsorbed contaminated carbon or minor surface oxidation because of the low O element content. After laser treatment, the relative area of C–O in both C1s and O1s spectra increase significantly, indicating that the femtosecond laser could induce the oxidation of PTFE. Despite the oxidation, the low-surface-energy C-F_2 and C-F_3 groups still dominate the surface after femtosecond laser processing.

The water droplets are spherical on the laser-structured surface [Fig. 2(i)], with a contact angle (CA) of 153.3 ± 0.4° [Fig. 2(j)]. The droplets can easily roll away with a sliding angle (SA) of 2.5 ± 0.3° [Fig. 2(k)]. Therefore, the laser-induced microstructure is superhydrophobic and has excellent water repellency. Superhydrophobicity is the result of the combined action of the intrinsic hydrophobicity of the PTFE substrate and the laser-induced microstructures.[27–29] This microstructure effectively reduces the contact area between water and the PTFE surface, so the droplet is in the Cassie state and only touches the peak portion of the textured surface, as shown in Fig. 2(m). In water, bubbles spread rapidly on the superhydrophobic surface within 7 ms, indicating that the superhydrophobic microstructure has excellent adsorption capacity for underwater gases, i.e., underwater superaerophilicity [Fig. 2(l)]. As shown in Fig. 2(n), the superhydrophobic surface microstructure cannot be wetted by water because of its water repellency. A trapped air layer is formed between the surface microstructure and the water environment. Once the bubble contacts the superhydrophobic surface, the gas inside the bubble will quickly enter the trapped air layer and diffuse out.

The femtosecond laser can also penetrate the PTFE film and produce perforated microholes using a point-by-point drilling method [Fig. 2(c)]. The laser is focused on the designed point, and a certain number of pulses are applied to ablate and penetrate the film. The laser focus then moves to the next point. Figure 2(e) shows an array of laser-drilled microholes on the PTFE film with a thickness of 0.2 mm. Each microhole is ablated with 100 laser pulses with a pulse energy of 200 μJ (Ω = 200 mW). The microholes have a diameter of 54.8 ± 0.4 μm and are uniformly distributed with a designed period of 80 μm. In addition, the inner walls of the perforated microholes are decorated with laser-induced micro/nanostructures, similar to the laser-ablated PTFE surface. By combining the laser-induced superhydrophobic surface microstructure with the laser-drilled microholes, a superhydrophobic porous film can be obtained [Figs. 2(f) and 2(g)]. The perforation of the laser-drilled microholes is verified by transmission microscope photography, as the backlight can pass through the microholes [Fig. 2(h)].

Laser processing parameters have important effects on the wettability of the laser-structured surface and the morphology of microholes.[30–32] Figure 3(a) shows the CA and SA values of water droplets on the PTFE surface ablated at different laser powers. As Ω increases from 20 to 50 mW, CA rapidly increases from 140.9 ± 0.6° to 153.3 ± 0.4°. The droplets cannot roll on the structured surface for Ω < 30 mW, even if the sample is upright (SA value is labeled 90°). The surface exhibits high water adhesion since such a low laser power cannot produce sufficient micro/nanostructures on the PTFE surface. At Ω = 50 mW, the ablated surface shows excellent superhydrophobicity with an SA of 2.5 ± 0.3°. As Ω continues to increase, the resultant surface remains superhydrophobic. Figure 3(b) shows the effect of laser scanning speed on wettability. At v = 5 mm/s, the ablated surface has a CA of 151.3 ± 0.1° and an SA of 10 ± 1.2°. When v increases from 10 to 35 mm/s, CA is greater than 150° and SA is less than 10°, indicating that the surface is superhydrophobic. The surface has a strong adhesion to water at v > 35 mm/s because the laser ablation point cannot

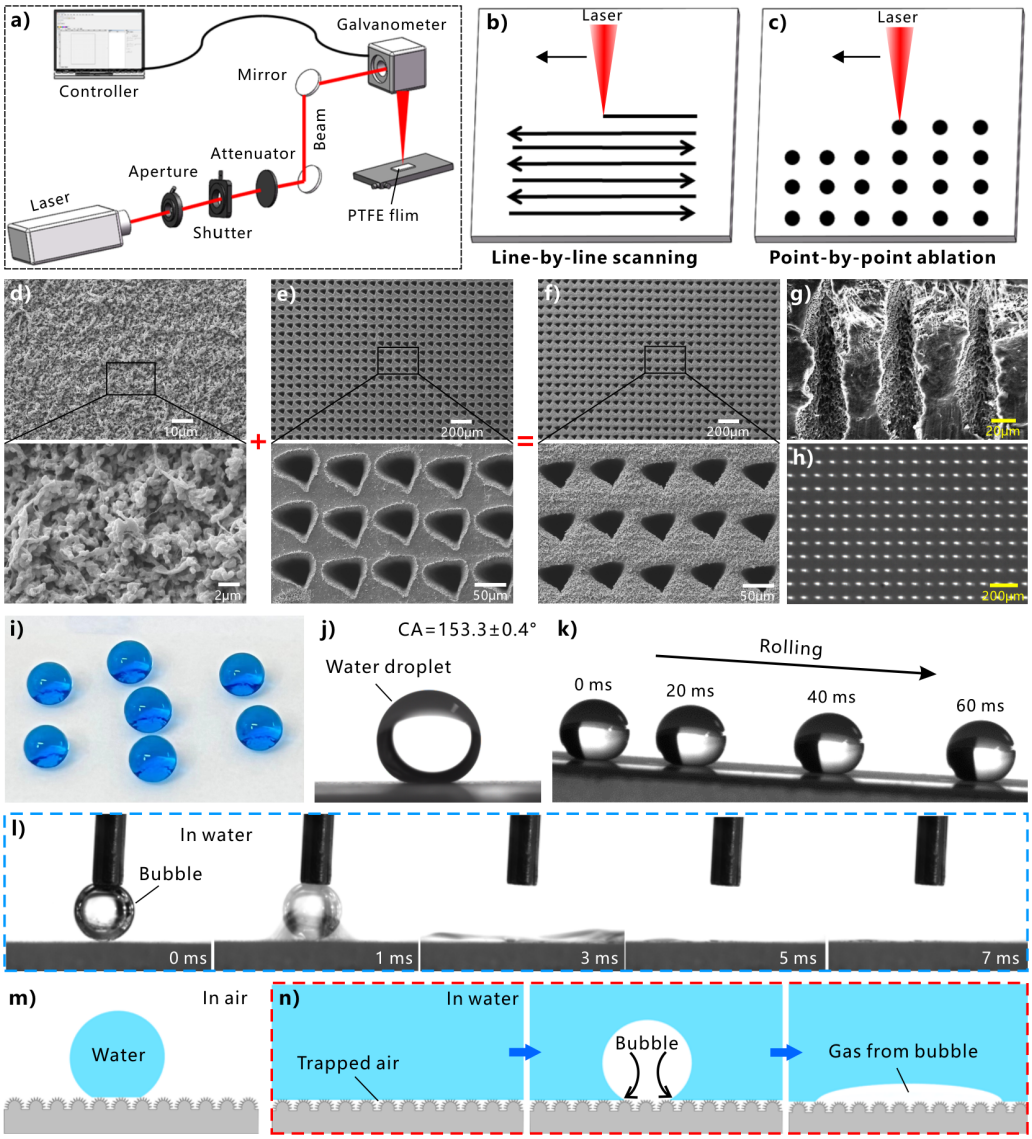

FIG. 2. Preparation of superhydrophobic porous PTFE films by a femtosecond laser. (a) Schematic diagram of the femtosecond laser processing system. (b) Line-by-line laser scanning. (c) Point-by-point laser ablation. SEM images of (d) the femtosecond laser-induced microstructure, (e) the laser-drilled perforated microholes, and (f) the resultant superhydrophobic porous microstructures. (g) Cross-sectional structure of the perforated microholes. (h) Transmission microscope photography of the porous film illuminated by a backlight. (i) Water droplets (blue color) and (j) droplet shape on the structured PTFE surface. (k) Process of droplet rolling on the inclined superhydrophobic surface. (l) Process of releasing a bubble onto the superhydrophobic surface in water. Formation mechanism of (m) superhydrophobicity and (n) underwater superaerophilicity of the laser-structured surface.

completely cover the PTFE surface during the too fast laser scanning process. Figure 3(c) shows the effect of the laser scanning space (Λ) on the wettability of the resultant microstructures. With increasing Λ, the CA value gradually decreases, and the SA value gradually increases. When Λ is small, the ablated regions of each scanning line overlap, which can completely cover the surface and form a uniform microstructure. In the range of $\Lambda \leq 20\ \mu$m, the surface is superhydrophobic, and the water adhesion is low. With increasing Λ, the laser-ablated regions of the scanning lines gradually separate, and nonablated domains appear between the adjacent scanning lines. The nonablated area leads to a gradual decrease in hydrophobicity.

Figures 3(d)–3(f) depicts the influence of laser processing parameters on the formation of perforated microholes. Too small Ω and too few pulses cannot ablate through the thin film. The experimental results show that open microholes can be formed on the PTFE film with a thickness of 0.2 mm only when Ω exceeds 50 mW and the laser pulse number exceeds 50 [Fig. 3(d)]. As shown in Fig. 3(e), the diameter of the generated microholes is positively correlated with Ω. As Ω

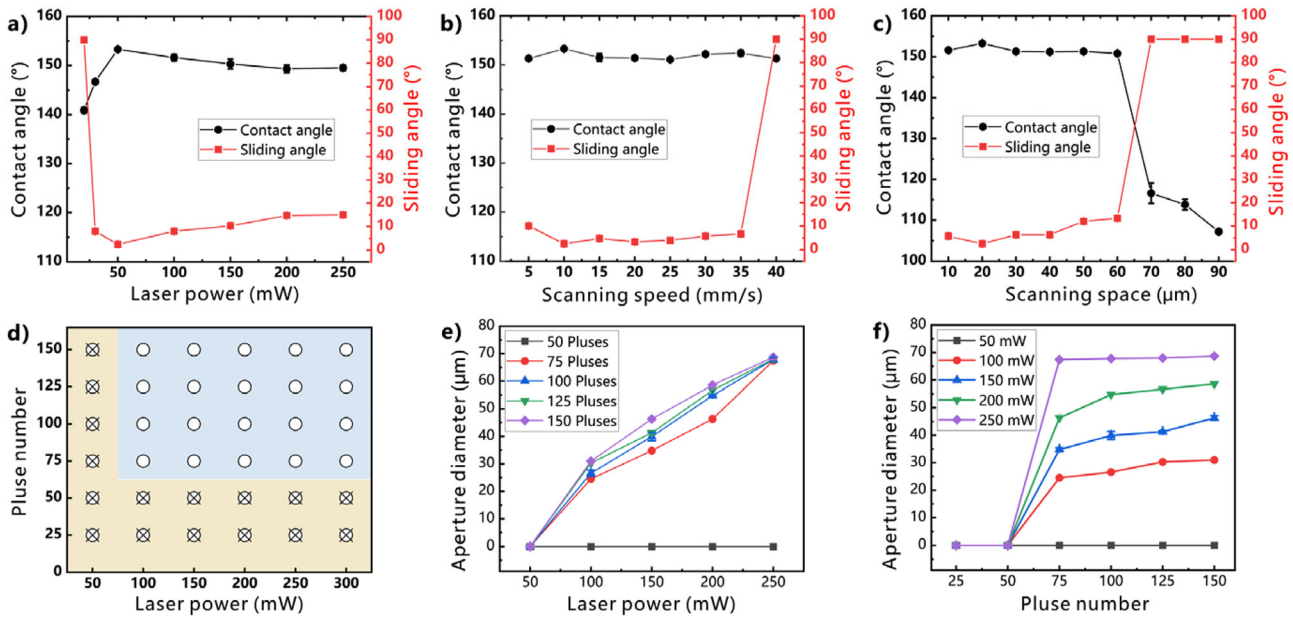

FIG. 3. Influence of laser processing parameters on wettability of the structured surface and morphology of the perforated microholes. Wettability of the surfaces prepared under different (a) laser powers (at $v = 10$ mm/s and $\Lambda = 20$ μm), (b) scanning speeds (at $\Omega = 50$ mW and $\Lambda = 20$ μm), and (c) scanning spaces (at $\Omega = 50$ mW and $v = 10$ mm/s). (d) Phase diagram of perforated microhole preparation: "○" means that the laser can ablate through the PTFE film and create open microholes, and "⊗" means that the film cannot be ablated through. Influence of the (e) laser power and (f) number of applied laser pulses on the diameter of the resultant perforated microholes.

increases from 50 to 250 mW, the diameter increases from 0 to 67.8 ± 0.7 μm (at 100 pulses). Similarly, the aperture diameter increases with the number of laser pulses [Fig. 3(f)]. As the pulse number increases from 50 to 75, the diameter rapidly increases from 0 to 46.3 ± 1.4 μm (at $\Omega = 200$ mW). If the pulse number continues to increase to 150, the diameter will slowly increase to 58.6 ± 0.9 μm.

The femtosecond laser-induced superhydrophobic surface microstructure and the microhole array can affect the discharge process of gas from water to the atmosphere environment. As shown in Fig. 4(a), an untreated PTFE film is placed on the water surface. When a bubble is released below the film, it will compete with the water attached to the PTFE surface. The bubble eventually forms a stable hemisphere on the untreated surface. Assuming a very small disturbance occurs, the energy change of the whole system can be expressed as [Fig. 4(b)] follows:[18,33,34]

$$\delta_w = \gamma_{SV} dA_{SV} + \gamma_{SL} dA_{SL} + \gamma_{LV} dA_{LV} + \Delta P dV, \quad (1)$$

where γ_{SV}, γ_{SL}, and γ_{LV} are the solid–vapor, solid–liquid, and liquid–vapor interfacial free energies, respectively; dA_{SV}, dA_{SL}, and dA_{LV} are the area changes of the solid–vapor, solid–liquid, and liquid–vapor interfaces, respectively; and ΔP and dV are the changes in Laplace pressure and gas volume, respectively. In the limited case of small perturbations, there are $dV = 0$, $dA_{SV} = -dA_{SL}$, and $dA_{LV}/dA_{SV} = \cos\theta$ for the hemispherical underwater bubbles (θ is the CA of the bubble). When equilibrium is reached, $\delta_W = 0$, so Eq. (1) can be simplified to

$$\cos\theta = \frac{\gamma_{SL} - \gamma_{SV}}{\gamma_{LV}}. \quad (2)$$

This equation describes the wettability of bubbles on the untreated PTFE surface. Since there are no perforated microholes in the untreated film, the bubbles cannot pass through the film and always stay in the water environment under the PTFE film.

Figure 4(c) shows the process of releasing a bubble under a porous PTFE film (without superhydrophobic surface microstructure). Within the first 6 ms, the wettability of the gas causes the bubble to rapidly expand outward, forming a hemisphere shape. As shown in Fig. 4(d), the internal pressure (P) of the bubble at this time is $P = P_0 + P_L + P_{water}$, where P_0 is the external atmospheric pressure, $P_L = \frac{2\gamma}{R}$ is the Laplace pressure caused by the bending of the water/gas interface (γ is the surface tension of water, R is the radius of curvature of the bubble), and P_{water} is the pressure caused by the water depth. In general, the Laplace pressure of small bubbles is greater than that of large bubbles. The bubble is connected to the atmosphere on the other side of the PTFE film through perforated microholes. There is a pressure difference between the gases on both sides of the film,[35,36]

$$\Delta P = P - P_0 = \frac{2\gamma}{R} + P_{water}. \quad (3)$$

This pressure difference drives the gas inside the bubble through the microholes and releases gas into the outside atmosphere. The bubble volume gradually decreases, and the bubble completely disappears at 62 ms. All the gas in the bubble passes through the porous film and is discharged into the atmosphere.

The superhydrophobic porous PTFE film has a strong adsorption capacity for bubbles in water. As shown in Fig. 4(e), when the bubble is in contact with the surface, the bubble can rapidly spread out under the film to form a large gas–solid contact area. The pressure difference between the bubble and the air environment also drives the gas in the bubble through the open microholes. Due to the larger contact area

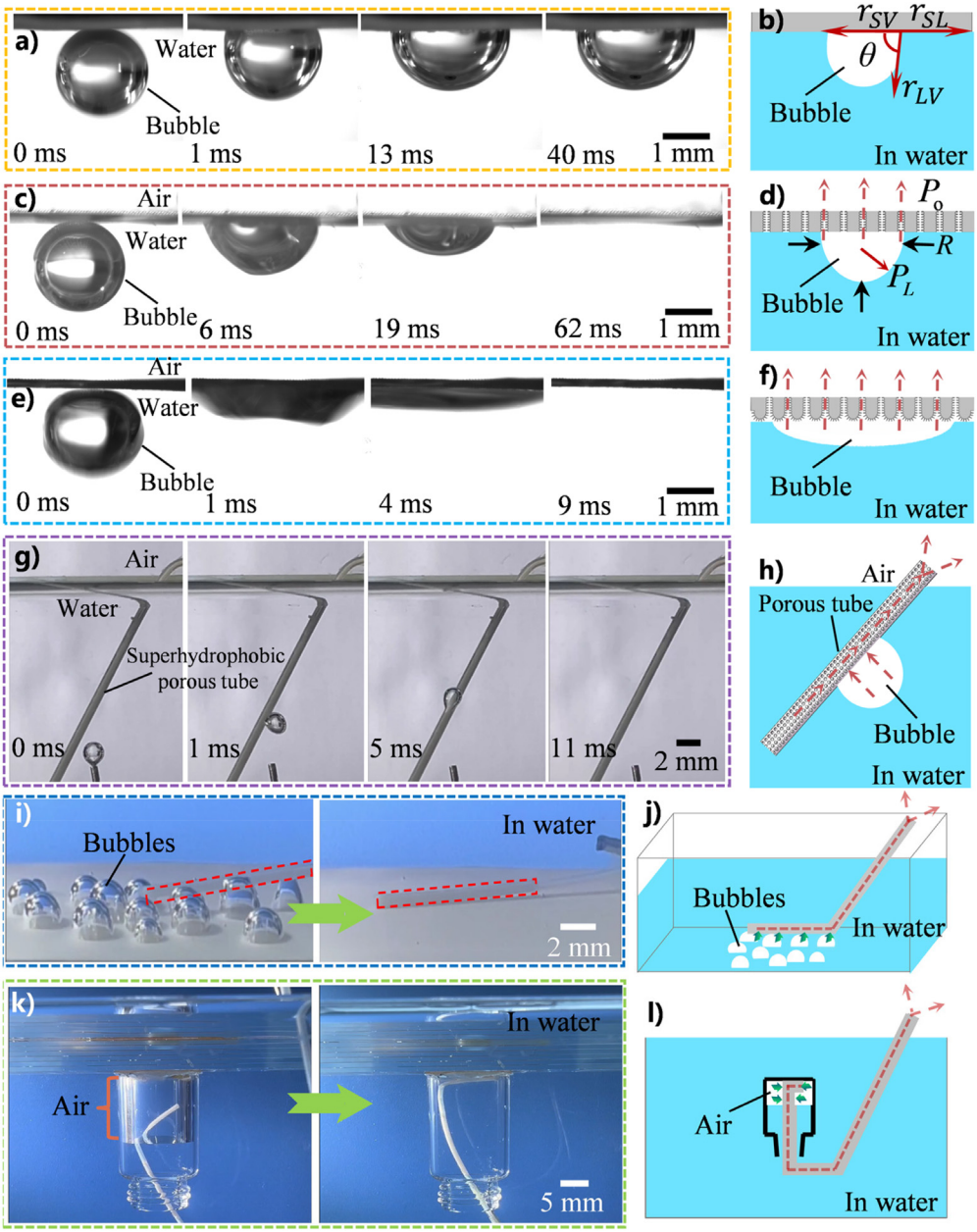

FIG. 4. Permeability of underwater bubbles through a superhydrophobic porous film. Releasing bubbles under different films floating on water: (a) and (b) an untreated flat PTFE film, (c) and (d) a porous PTFE film without superhydrophobic surface microstructure, and (e) and (f) a superhydrophobic porous PTFE film. (g) and (h) Process of absorbing an underwater bubble through a superhydrophobic porous thin tube and releasing gas into the air. (b), (d), (f), and (h) are the corresponding schematic diagrams of (a), (c), (e), and (g). (i) and (j) The process of absorbing air bubbles at the bottom of a container through a superhydrophobic porous tube and releasing gas into the air. (k) and (l) The process of absorbing an air pocket at the bottom of an underwater inverted container through a superhydrophobic porous tube and releasing it into the air.

between the bubble and the porous film, there are more open microholes for gas transport [Fig. 4(f)]. The gas in the bubble can be completely released into the atmosphere within 9 ms. The discharge rate of gas is approximately seven times that of the common porous film. The experimental results demonstrate that a superhydrophobic surface microstructure and perforated microholes are key to gas discharge. Perforated microholes provide microchannels for underwater bubbles to access the external environment. The superhydrophobic microstructure significantly increases the number of microholes covered by underwater gas, thus promoting the rapid passage of gas

through the porous film. In addition, the superhydrophobicity of the surface microstructure and microholes prevents water from passing through the porous structure.

In the process of gas discharge, the underwater bubbles first integrate into the gas film on the superhydrophobic surface, and then release into the atmosphere through perforated microholes [Fig. S2(a) in the supplementary material]. Regardless of how large or small the bubble is in contact with the gas film, it can be easily adsorbed by the gas film, so, theoretically, any volume of bubbles can be removed. For example, underwater bubbles as small as 200 nl and as large as 0.6 ml can be discharged into the atmosphere through the superhydrophobic porous film [Figs. S2(b) and S2(c) in the supplementary material]. The diameter and density of the microholes only affect the rate of gas removal. The inherent chemical inertness of PTFE makes the superhydrophobicity of the femtosecond laser-induced microstructures very stable and even resistant to corrosion of various corrosive liquids.[37,38] Even if the superhydrophobic PTFE surface and the superhydrophobic porous film are stored in air or submerged in water for ten days, the superhydrophobicity is almost unchanged [Figs. S3(a) and S3(b) in the supplementary material], and the porous film can still discharge bubbles normally [Figs. S3(c) and S3(d) in the supplementary material]. The durability is much longer than the infusion time (usually within two hours), ensuring the normal use in the infusion process.

Superhydrophobic porous microstructures can release gases from water into the air environment. By preparing superhydrophobic microstructures and microholes on the wall of a PTFE tube with a diameter of 1.2 mm, a superhydrophobic porous thin tube is obtained. When one end of the tube is inserted into the water, the space inside the tube is connected to the outside air. As shown in Fig. 4(g), an underwater bubble can be rapidly absorbed by the fine tube within 11 ms. The adsorbed gas is then released into the atmosphere along the inserted tube [Fig. 4(h), Movie S1]. In some cases, bubbles cannot spontaneously rise into the air, such as bubbles attached to the sidewall or bottom of a container. We can move the superhydrophobic porous tube into contact with the bubbles, which allows the bubbles to be quickly absorbed and released into the atmosphere [Figs. 4(i) and 4(j), Movie S2]. To remove the air pocket in the underwater cavity, a curved superhydrophobic porous tube is inserted in the air pocket portion so that the gas is transported along the gas pipe to the external environment [Figs. 4(k) and 4(l), Movie S3].

The ability of superhydrophobic porous tubes to absorb and discharge gas also enables them to be used to remove bubbles from water flow in pipes. As a demonstration, Fig. 5 shows a strategy for eliminating bubbles in an infusion tube using a superhydrophobic porous thin tube. The thin tube only needs to be inserted into the infusion tube. When bubbles appear, they flow forward with the water flow [Fig. 5(a)]. Once the bubble comes into contact with the inserted thin tube, the pressure inside the bubble will force the gas in the bubble through the microholes into the superhydrophobic tube. Since the other end of the inserted tube faces the external environment, the absorbed gas can be transported along the tube and released into the atmosphere [Figs. 5(b) and 5(c)]. As the bubble moves forward, the gas inside the bubble will continue into the gas tube and out of the infusion tube (Movie S4). Finally, the entire bubble can be completely removed.

In summary, the effective removal of bubbles in water by combining superhydrophobic surface microstructures and perforated microholes is demonstrated. Superhydrophobic porous microstructures are prepared on PTFE thin films or tubes by femtosecond laser processing. The superhydrophobic porous film can absorb bubbles in water and allow gas bubbles to pass through the film to the air environment

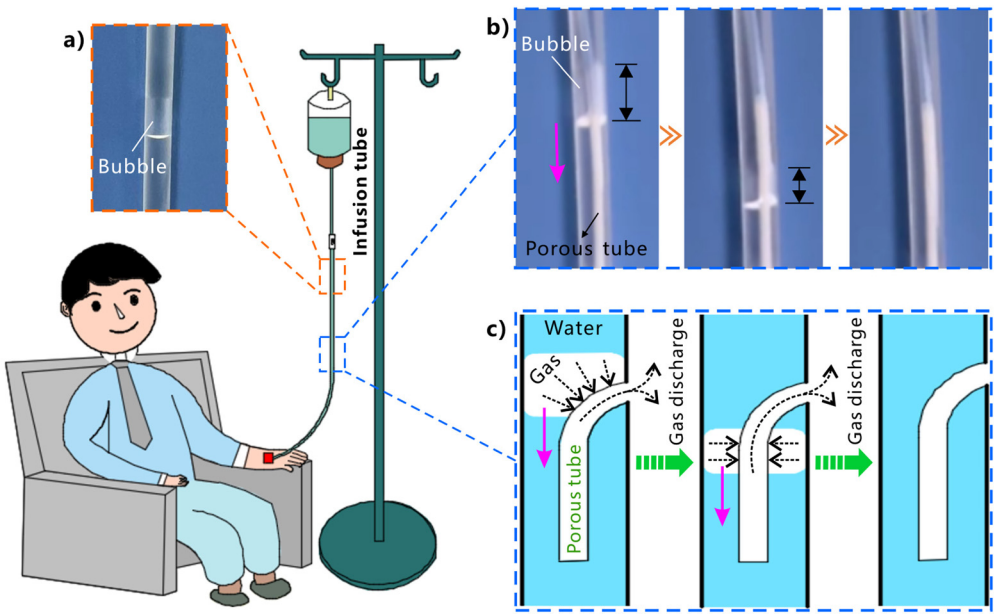

FIG. 5. Removal of bubbles from an infusion tube based on an inserted superhydrophobic porous thin tube. (a) Bubble in the infusion tube moving forward with the water flow. (b) The process of bubble removal and (c) the corresponding schematic diagrams: (1) the bubble touching the inserted superhydrophobic porous tube (left images), (2) decrease in the bubble volume as the gas enters the inserted tube (middle images), and (3) after the bubble is completely discharged (right images).

under the drive of Laplace pressure and underwater pressure. The gas discharge rate of the superhydrophobic porous film is about seven times that of the ordinary porous film. An effective strategy to remove bubbles in an infusion tube by inserting superhydrophobic porous thin tubes is proposed. The whole bubble can be completely discharged out of the infusion tube. This method has important potential applications in microfluidics, biomedicine, chemical manufacturing, and other fields and can effectively avoid the harm caused by tiny bubbles.

See the supplementary material for the chemical change after laser ablation, the discharge of 200 nl and 0.6 ml bubbles, the durability of the superhydrophobicity, and the movies of the dynamic process of adsorbing underwater bubbles.

This work was supported by the USTC Research Funds of the Double First-Class Initiative (No. YD2090002013) and the Natural Science Foundation of Anhui Province (No. 1908085ME130).

AUTHOR DECLARATIONS

Conflict of Interest

The authors have no conflicts to disclose.

Author Contributions

Yansheng Yao: Conceptualization (equal); Data curation (equal); Funding acquisition (equal); Resources (equal); Writing – review & editing (equal). **Qiangsong Meng:** Data curation (equal); Investigation (equal); Writing – original draft (equal). **Yubin Peng:** Data curation (equal); Resources (equal); Supervision (equal). **Zilong Cheng:** Investigation (equal). **Xinlei Li:** Investigation (equal). **Tianyu Xu:** Investigation (equal). **Jiale Yong:** Conceptualization (equal); Funding acquisition (equal); Resources (equal); Supervision (equal).

DATA AVAILABILITY

The data that support the findings of this study are available from the corresponding authors upon reasonable request.

REFERENCES

[1]X. Li, J. Zhang, X. Wang *et al.*, "Bio-inspired spontaneous splitting of underwater bubbles along a superhydrophobic open pathway without perturbation," Droplet **1**, 65–75 (2022).
[2]X. Yan, W. Xu, Y. Deng *et al.*, "Bubble energy generator," Sci. Adv. **8**, eabo7698 (2022).
[3]A. Azevedo, H. Oliveira, and J. Rubio, "Bulk nanobubbles in the mineral and environmental areas: Updating research and applications," Adv. Colloid Interface Sci. **271**, 101992 (2019).
[4]I. Levitsky, D. Tavor, and V. Gitis, "Micro and nanobubbles in water and wastewater treatment: A state-of-the-art review," J. Water Process. Eng. **47**, 102688 (2022).
[5]I. Pereiro, A. F. Khartchenko, L. Petrini *et al.*, "Nip the bubble in the bud: A guide to avoid gas nucleation in microfluidics," Lab Chip **19**, 2296–2314 (2019).
[6]X. Zhao, C. Ma, D. S. Park *et al.*, "Air bubble removal: Wettability contrast enabled microfluidic interconnects," Sens. Actuators, B **361**, 131687 (2022).
[7]A. Angulo, P. van der Linde, H. Gardeniers *et al.*, "Influence of bubbles on the energy conversion efficiency of electrochemical reactors," Joule **4**, 555–579 (2020).
[8]B. Liu, R. Manica, Q. Liu *et al.*, "Coalescence of bubbles with mobile interfaces in water," Phys. Rev. Lett. **122**, 194501 (2019).
[9]Y. Pang, Y. Lu, X. Wang *et al.*, "Impact of flow feedback on bubble generation in T-junction microchannels under pressure-driven condition," Chem. Eng. Sci. **246**, 117010 (2021).
[10]K. K. Wong and K. C. Leong, "Saturated pool boiling enhancement using porous lattice structures produced by selective laser melting," Int. J. Heat Mass Transfer **121**, 46–63 (2018).
[11]S. Al-Afif, H. Elkayekh, M. Omer *et al.*, "Analysis of risk factors for venous air embolism in the semisitting position and its impact on outcome in a consecutive series of 740 patients," J. Neurosurg. **137**, 258–265 (2022).
[12]M. A. Mirski, A. V. Lele, L. Fitzsimmons *et al.*, "Diagnosis and treatment of vascular air embolism," Anesthesiology **106**, 164–177 (2007).
[13]V. Monnin-Bares, G. Chassagnon, H. Vernhet-Kovacsik *et al.*, "Systemic air embolism depicted on systematic whole thoracic CT acquisition after percutaneous lung biopsy: Incidence and risk factors," Eur. J. Radiol. **117**, 26–32 (2019).
[14]X. He, B. Wang, J. Meng *et al.*, "How to prevent bubbles in microfluidic channels," Langmuir **37**, 2187–2194 (2021).
[15]J. Song, Z. Liu, X. Wang *et al.*, "High-efficiency bubble transportation in an aqueous environment on a serial wedge-shaped wettability pattern," J. Mater. Chem. A **7**, 13567–13576 (2019).
[16]L. Yan, X. Yang, Y. Zhang *et al.*, "Porous Janus materials with unique asymmetries and functionality," Mater. Today **51**, 626–647 (2021).
[17]Z. Xiao, D. Li, Q. Zhu *et al.*, "Simultaneous removal of NO and SO_2 through a new wet recycling oxidation–reduction process utilizing micro-nano bubble gas–liquid dispersion system based on Na_2SO_3," Fuel **263**, 116682 (2020).
[18]J. Yong, F. Chen, Y. Fang *et al.*, "Bioinspired design of underwater superaerophobic and superaerophilic surfaces by femtosecond laser ablation for anti- or capturing bubbles," ACS Appl. Mater. Interfaces **9**, 39863–39871 (2017).
[19]J. Yong, F. Chen, W. Li *et al.*, "Underwater superaerophobic and superaerophilic nanoneedles-structured meshes for water/bubbles separation: Removing or collecting gas bubbles in water," Global Challenges **2**, 1700133 (2018).
[20]J. Yong, F. Chen, J. Huo *et al.*, "Femtosecond laser induced underwater superaerophilic and superaerophobic PDMS sheets with through microholes for selective passage of air bubbles and further collection of underwater gas," Nanoscale **10**, 3688–3696 (2018).
[21]J. Yong, Q. Yang, J. Huo *et al.*, "Underwater gas self-transportation along femtosecond laser-written open superhydrophobic surface microchannels (<100 μm) for bubble/gas manipulation," Int. J. Extreme Manuf. **4**, 015002 (2022).
[22]A. Kannan, P. Hristov, J. Li *et al.*, "Surfactant-laden bubble dynamics under porous polymer films," J. Colloid Interface Sci. **575**, 298–305 (2020).
[23]K. K. Lay, J. S. Ong, K. Y. Yong *et al.*, "Nucleate pool boiling enhancement by ultrafast water permeation in graphene-nanostructure," Int. Commun. Heat Mass Transfer **101**, 26–34 (2019).
[24]X. Chen and M. Gu, "Two-beam ultrafast laser scribing of graphene patterns with 90-nm subdiffraction feature size," Ultrafast Sci. **2022**, 0001.
[25]D. Zhang, R. Liu, and Z. Li, "Irregular LIPSS produced on metals by single linearly polarized femtosecond laser," Int. J. Extreme Manuf. **4**, 015102 (2022).
[26]L. Zhu, Y.-L. Zhang, and H.-B. Sun, "Miniaturising artificial compound eyes based on advanced micronanofabrication techniques," Light: Sci. Appl. **2**, 84–100 (2021).
[27]J. Yong, S. C. Singh, Z. Zhan *et al.*, "Substrate-independent, fast, and reversible switching between underwater superaerophobicity and aerophilicity on the femtosecond laser-induced superhydrophobic surfaces for selectively repelling or capturing bubbles in water," ACS Appl. Mater. Interfaces **11**, 8667–8675 (2019).
[28]J. Yong, Q. Yang, X. Hou *et al.*, "Nature-inspired superwettability achieved by femtosecond lasers," Ultrafast Sci. **2022**, 9895418.
[29]Y. Zhan, S. Yu, A. Amirfazli *et al.*, "Preparations of versatile polytetrafluoroethylene superhydrophobic surfaces using the femtosecond laser technology," Colloids Surf., A **629**, 127441 (2021).
[30]S. Liu, G. Xiao, O. Lin *et al.*, "A new one-step approach for the fabrication of microgrooves on Inconel 718 surface with microporous structure and nanoparticles having ultrahigh adhesion and anisotropic wettability: Laser belt processing," Appl. Surf. Sci. **607**, 155108 (2023).
[31]Q. Wang, P. Yao, Y. Li *et al.*, "Inverted pyramid structure on monocrystalline silicon processed by wet etching after femtosecond laser machining in air and deionized water," Opt. Laser Technol. **157**, 108647 (2023).

[32]W. Zhang, P. Zhang, H. Yan *et al.*, "Research status of femtosecond lasers and nanosecond lasers processing on bulk metallic glasses (BMGs)," Opt. Laser Technol. **167**, 109812 (2023).
[33]Y. Xiao, J. Zheng, Y. He *et al.*, "Droplet and bubble wetting behaviors: The roles of surface wettability and roughness," Colloids Surf., A **653**, 130008 (2022).
[34]J. Yong, Y. Peng, X. Wang *et al.*, "Self-driving underwater 'aerofluidics,'" Adv. Sci. **10**, 2301175 (2023).
[35]W. Li, J. Zhang, Z. Xue *et al.*, "Spontaneous and directional bubble transport on porous copper wires with complex shapes in aqueous media," ACS Appl. Mater. Interfaces **10**, 3076–3081 (2018).
[36]Y. Xing, X. Gui, and Y. Cao, "Effects of bubble size and approach velocity on bubble–particle interaction—A theoretical study," J. Dispersion Sci. Technol. **39**, 929–933 (2018).
[37]Y. Fang, J. Yong, F. Chen *et al.*, "Durability of the tunable adhesive superhydrophobic PTFE surfaces for harsh environment applications," Appl. Phys. A **122**, 827 (2016).
[38]J. Yong, Y. Fang, F. Chen *et al.*, "Femtosecond laser ablated durable superhydrophobic PTFE films with micro-through-holes for oil/water separation: Separating oil from water and corrosive solutions," Appl. Surf. Sci. **389**, 1148–1155 (2016).